

NIERT: Accurate Numerical Interpolation through Unifying Scattered Data Representations using Transformer Encoder

Shizhe Ding, Boyang Xia, Milong Ren, Dongbo Bu

Abstract—Interpolation for scattered data is a classical problem in numerical analysis, with a long history of theoretical and practical contributions. Recent advances have utilized deep neural networks to construct interpolators, exhibiting excellent and generalizable performance. However, they still fall short in two aspects: **1) inadequate representation learning**, resulting from separate embeddings of observed and target points in popular encoder-decoder frameworks and **2) limited generalization power**, caused by overlooking prior interpolation knowledge shared across different domains. To overcome these limitations, we present a **Numerical Interpolation** approach using **Encoder Representation of Transformers** (called **NIERT**). On one hand, NIERT utilizes an encoder-only framework rather than the encoder-decoder structure. This way, NIERT can embed observed and target points into a unified encoder representation space, thus effectively exploiting the correlations among them and obtaining more precise representations. On the other hand, we propose to pre-train NIERT on large-scale synthetic mathematical functions to acquire prior interpolation knowledge, and transfer it to multiple interpolation domains with consistent performance gain. On both synthetic and real-world datasets, NIERT outperforms the existing approaches by a large margin, i.e., $4.3\sim 14.3\times$ lower MAE on TFRD subsets, and $1.7/1.8/8.7\times$ lower MSE on Mathit/PhysioNet/PTV datasets. The source code of NIERT is available at <https://github.com/DingShizhe/NIERT>.

Index Terms—Interpolation algorithm, scattered data, Transformer encoder, pre-trained models.



1 INTRODUCTION

SCATTERED data refers to a set of points and their corresponding values, in which the points lack structured relationships beyond their relative positions [1]. Such data commonly arise in a wide range of theoretical and practical scenarios, including solving partial differential equations (PDEs) [1], [2], temperature field reconstruction [3], particle tracking velocimetry [4], and irregularly-sampled time series analysis [5], [6] (Fig. 1a). Numerical interpolation is often required for scattered data, which involves estimating values for target points based on the exact values at some observed points. For instance, in temperature field reconstruction for micro-scale electronics, interpolation methods are employed to obtain real-time working environments for electronic components from limited measurements, and inaccurate interpolation can significantly increase the cost of predictive maintenance. Therefore, accurate numerical interpolation approaches are highly desirable.

A large number of approaches have been proposed for interpolating scattered data. Traditional approaches utilize a linear combination of pre-defined basis functions to ap-

proximate the target function, as demonstrated in Figure 1b [7]. To adapt to different scenarios, various types of basis functions have been devised. For example, the spline interpolation algorithm uses polynomials of a small degree over subintervals of the approximation domain as basis functions, and the RBF interpolation algorithm uses radial basis functions. Most of these schemes can theoretically guarantee interpolation accuracy when sufficient observed points are available; however, they have also been shown to be ineffective for sparse data points or complex functions [8]. Furthermore, these methods are inherently not learning-based, *i.e.*, they cannot take advantage of data from the same function distribution, which limits their generalizability and interpolation accuracy.

Recent advances have exhibited an alternative strategy that uses neural networks to learn target functions from the given observed points. For example, conditional neural processes (CNPs) [9] and their extensions [10], [11], [12] use neural networks to model the conditional distribution of regression functions given the observed points, and [3] proposed to use Transformer [13] to solve interpolation tasks in temperature field reconstruction. Unlike traditional approaches that directly output explicit target functions, these neural models take the observed points and target points' locations as input, and estimate the values of these target points. Thus, it is reasonable to view this task as a set-to-set task, which motivates all of these models to employ encoder-decoder structures (Fig. 1c). The encoder here embeds the observed points to a latent space while the decoder estimates values for target points. Compared with the traditional approaches, these learning-based methods can learn the function distribution as well as the correlation

- Shizhe Ding, Boyang Xia, Milong Ren are with Key Lab of Intelligent Information Processing of Chinese Academy of Sciences (CAS), Institute of Computing Technology, CAS, Beijing 100190, China, and University of Chinese Academy of Sciences, Beijing 100049, China.
E-mail: {dingshizhe19s, xiaboyang20s, renmilong21b}@ict.ac.cn
- Dongbo Bu is with Key Lab of Intelligent Information Processing of Chinese Academy of Sciences (CAS), Institute of Computing Technology, CAS, Beijing 100190, China, University of Chinese Academy of Sciences, Beijing 100049, China, and Zhongke Big Data Academy, Zhengzhou 450046, China.
E-mail: dbu@ict.ac.cn
- Corresponding Author: Dongbo Bu

Manuscript received March 8, 2022.

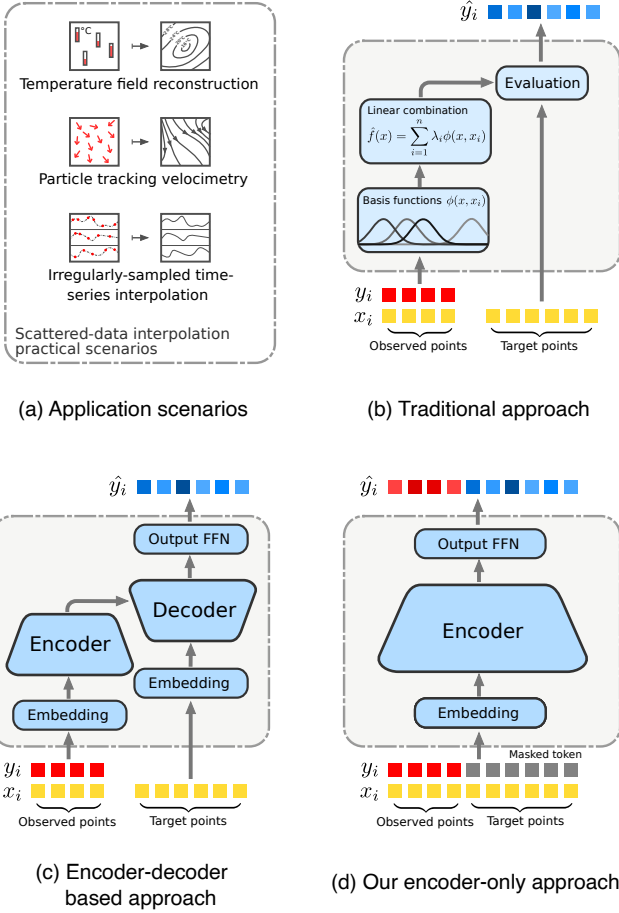


Fig. 1. Application scenarios of scattered data interpolation, and comparison of existing approaches with our NIERT approach. (a) Various scenarios of scattered data interpolation. (b) The traditional approaches output explicit target functions expressed as a linear combination of basis functions. (c) In the encoder-decoder framework, the encoder and decoder process observed points and target points in a separate fashion, which results in inadequate representation learning. (d) Our encoder-only framework processes observed and target points in a unified fashion, which helps obtain more precise target point representations.

among scattered points from existing datasets and generalize to new interpolation tasks, which significantly improves the interpolation accuracy.

Despite the excellent performance of existing learning-based interpolation models for scattered data, they still fall short in two aspects: **1) overlooking the homogeneity of observed and target points**, which leads to inadequate representation learning of scattered points, and **2) lack of prior interpolation knowledge**, which leads to limited generalization power. The underlying reasons of these limitations are: First, the encoder-decoder-based models process the observed and target points in the encoder and decoder separately, which keeps their learned representations in different feature spaces. However, the observed points and target points are intrinsically homogeneous, *i.e.*, they are all sampled from the same function. Treating observed and target points separately may hinder the transfer of information from observed points to target points and increase the difficulty of learning the correlations between the observed points and target points. This strategy makes the represen-

tation of target points not precise enough, which limits the final interpolation accuracy.

Second, another shortcoming of these learning-based interpolation models is the lack of prior interpolation knowledge. The continuity and smoothness of the target function are always considered in traditional scattered data interpolation algorithms, *e.g.*, using smooth basis functions to obtain smooth target functions [1]. This prior knowledge reflects the general properties of the function distribution, effectively narrowing the potential range of the target function and guaranteeing interpolation accuracy [7]. However, these existing neural interpolators lack such prior knowledge since they learn interpolation knowledge only from a domain-specific scattered dataset. This makes them lack generalization power to various domains.

To address these limitations, we propose a highly-accurate learning-based numerical interpolation approach for scattered data, which can effectively learn precise point representations with high generalization power. The basic ideas of our approach is as follows: First, to obtain more precise representations of the target points, we propose a novel interpolation model, called NIERT, which uses a transformer-based encoder-only structure rather than popular encode-decoder structures. Different from previous works, NIERT processes both observed and target points in a unified fashion (see Fig. 1d). To bridge the gap between target points and observed points, *i.e.*, to address the missing values of target points, we augment target points with learnable mask tokens, which is similar to BERT [14]. Then we feed them into the encoder together with the observed points. This design improves modeling the correlations between these two types of points, which yields more precise representations and improves interpolation interpretability¹. Moreover, to prevent the unexpected interference posed by target points on the observed points, we introduce a partial self-attention mechanism to calculate attention among the given data points except for the influence of target points on the observed points at each layer. This further boosts interpolation robustness.

Second, we use the pre-training technique to incorporate the prior interpolation knowledge into our NIERT interpolator, which has been successfully used for representation learning [14], [15]. The key step towards this goal is building a task set for scattered-data interpolation with rich prior interpolation knowledge. For this purpose, we synthesized a large number of symbolic mathematical functions and generated a new task set by sampling from these functions. Large-scale syntheses of mathematical functions have the potential to cover real-world continuous and smooth functions in many domains at low cost. With this enhancement, the pre-trained NIERT interpolators can be easily transferred to a variety of domain-specific tasks with a lower learning difficulty and higher interpolation accuracy.

The main contributions of this study are summarized as follows.

- We design a transformer-based encoder-only interpolation framework and embed the observed and

¹ The higher “interpretability” here means more visually reasonable correlations between observed and target points (See Sec. 5.3 for details.)

target points into a unified feature space, to obtain more accurate target point representations. Also, we propose a partial self-attention mechanism with a strong inductive bias for interpolation tasks, to avoid the interference of one type of points onto the others, which also boosts robustness.

- We leverage the pre-training technique to improve the generalization power of interpolation models. We synthesize a large-scale interpolation task set by generating a massive amount of symbolic mathematical functions. To the best of our knowledge, this study is the first work to propose the pre-trained models for scatter-data interpolation.
- Our approach significantly outperforms both state-of-the-art learning-based approaches and traditional approaches on 4 synthetic and real-world datasets in terms of both interpolation accuracy and interpretability, which shows the potential of our approach in a wide range of application fields.

The paper is structured as follows: Section 2 provides a literature review. Section 3 presents our approach. Section 4 elaborates on the experimental setup. Section 4 reports experimental results and analysis. Section 6 discusses the connections between our approach and traditional interpolation methods. Finally, Section 7 draws conclusions.

2 RELATED WORKS

2.1 Traditional interpolation approaches for scattered data

Traditional interpolation approaches for scattered data construct interpolation functions through combining explicitly pre-defined basis functions. The representative approaches include Lagrange interpolation, Newton interpolation [7], B-spline interpolation [16], Shepard’s method [17], Kriging [18], and radial basis function interpolation (RBF) [19], [20]. Among these approaches, the classical Lagrange interpolation, Newton interpolation and B-splines interpolation are usually used for univariate interpolation. [21] proposed a high-order multivariate approximation scheme for scattered data sets, in which approximation error is represented using Taylor expansions at data points, and basis functions are determined by minimizing the approximation error.

2.2 Neural network-based interpolation approaches

Equipped with deep neural networks, data-driven interpolation and reconstruction methods show great advantages and potential. For instance, convolutional neural networks (CNNs) have been applied in the interpolation tasks of single image super-resolution [22], [23], and recurrent neural networks (RNNs) and Transformers have been used for interpolation of sequences like time series data [6], [24].

Recently, [9] proposed to model the conditional distribution of regression functions given observed points. The proposed approach, called conditional neural processes (CNPs), has shown increased estimation accuracy and generalizing ability. A variety of studies have been performed to enhance CNPs: [10] designed attentive neural processes (ANPs), which shows improved accuracy. [12] leveraged Bayesian last layer (BLL) [25] for faster training and better

prediction. In addition, the bootstrap technique was also employed for further improvement [11]. To solve the interpolation task in 2D temperature field reconstruction, [3] proposed a Transformer-based approach, referred to as TFR-transformer, which can also be applied to solve interpolation tasks for scattered data with higher dimensions.

2.3 Masked language/image models and the pre-training technique

The design of NIERT is also inspired by the recent advances in masked language/image models [14], [15], [26], [27] and pre-trained models for symbolic regression [28], [29]. The mask mechanism enables the models to reconstruct missing data from their context and effectively learn representations of language and images. As a way of introducing prior knowledge, large-scale pre-training allows language or visual models to acquire more general text or image representation capabilities, which assists the learning process on downstream tasks and significantly improves their performance. In addition, the pre-trained models for symbolic regression were designed to learn the map from scattered data to corresponding symbolic formulas [28], [29]. Here, NIERT uses the mask mechanism to reconstruct the missing values of target points and uses the pre-training technique to acquire strong generalization power.

3 METHOD

3.1 Overview of NIERT approach

In the study, we focus on the interpolation task that can be formally described as follows: We are given n observed points with known values $O = \{(x_i, y_i)\}_{i=1}^n$, and m target points with values to be determined, denoted as $T = \{x_i\}_{i=n+1}^{n+m}$. Here, $x_i \in \mathbb{R}^{d_x}$ denotes the position of a point, $y_i = f(x_i) \in \mathbb{R}^{d_y}$ denotes the value of a point, and $f : \mathbb{R}^{d_x} \rightarrow \mathbb{R}^{d_y}$ denotes a function mapping positions to values. The d_x and d_y denote the dimension of a point’s position and the dimension of the value, respectively. The function f is from a function distribution \mathcal{F} , which can be explicitly defined using a mathematical formula or implicitly represented using a set of scattered data in the form (x_i, y_i) . The goal of the interpolation task is to accurately estimate the values $f(x)$ for each target point $x \in T$ according to the observed points in O .

The main element of our NIERT approach is a neural interpolator that learns to estimate values for target points. We train the neural interpolator using a set of interpolation tasks sampled from the function distribution \mathcal{F} (Sec. 3.2 and Fig. 2). For each of the sampled interpolation tasks, we mask the values of target points, feed the task to the neural interpolator, and train the interpolator to predict the values of target points and observed points as well. The training objective is to minimize the error between the predicted values and the ground-truth values of both target and observed points. The trained interpolator can be used to interpolate values of target points for the interpolation tasks from the distribution \mathcal{F} . In addition, to enable NIERT with generalization power to various interpolation domains, we pre-train NIERT on a large-scale interpolation task set **Mathit**, which we generate by sampling on synthesized

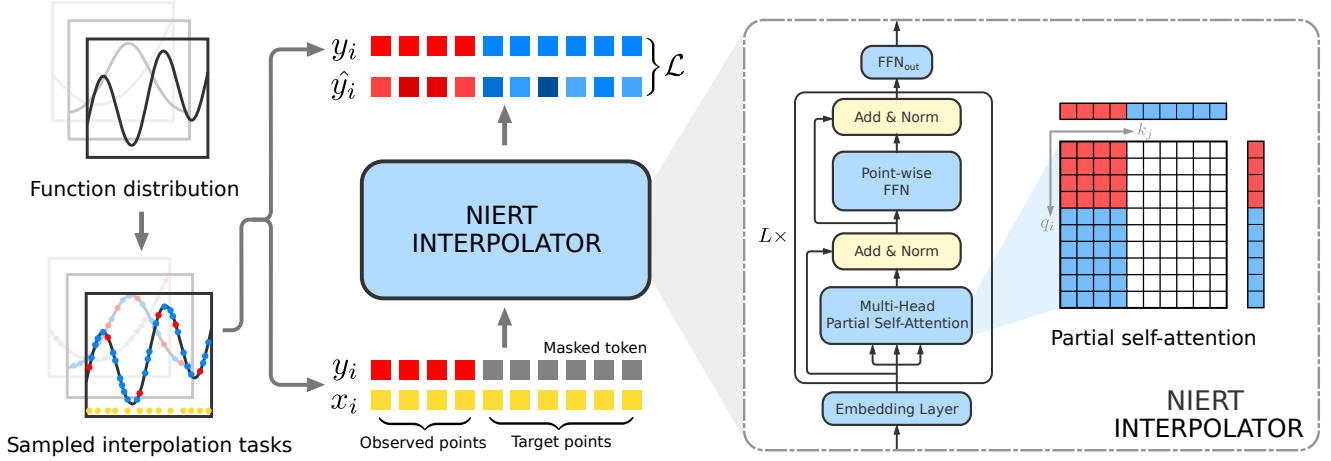


Fig. 2. Overview of NIERT training process. Here, x_i represents the position of a point, and y_i represents its value. The predicted values of the point is denoted as \hat{y}_i . We prepare the training interpolation tasks by first sampling functions from a function distribution \mathcal{F} and then sampling observed points O and target points T on each function. NIERT trains an interpolator over this data. The partial self-attention mechanism facilitates exploiting the correlations between observed points and target points and avoiding the unexpected interference of target points on observed points.

mathematical symbolic functions (see Sec. 3.3 and Fig. 3). In the following sections, we first present the NIERT encoder-only structure, then we introduce the pre-training technique.

3.2 Architecture of the NIERT interpolator

The neural interpolator in NIERT adopts the Transformer encoder framework; however, to suit the interpolation task, significant modifications and extensions were made in the embedding, Transformer and output layers, which are described in detail below.

Unified representations with masked tokens. NIERT embeds both observed points and target points into the unified high-dimensional embedding space. As the position x of a data point and its value y are from different domains, we use two linear modules: Linear_x embeds the positions while Linear_y embeds the values.

We feed the points and target points into the same embedding modules $\text{Linear}_x, \text{Linear}_y$. It should be noted that for target points, their values are absent when embedding as they are to be determined. In this case, we use a masked token as a substitute, which is embedded as a trainable parameter MASK_y as performed in BERT [14]. This way, the interpolator processes both target points and observed points in a unified fashion.

We concatenate the embeddings of position and value of a data point as the point's embedding, denoted as h_i^0 , i.e.,

$$h_i^0 = \begin{cases} [\text{Linear}_x(x_i), \text{Linear}_y(y_i)], & \text{if } (x_i, y_i) \in O \\ [\text{Linear}_x(x_i), \text{MASK}_y], & \text{if } x_i \in T \end{cases}$$

Partial self-attention mechanism. NIERT feeds the embeddings of the points into a stack of L Transformer layers, producing encodings of these points as result. Through the l -th layer, the encoding of the i -th point h_i^l are transformed to h_i^{l+1} . Each Transformer layer contains two subsequent sub-layers, namely, a multi-head partial self-attention module, and a point-wise fully-connected network. These sub-layers are interlaced with residual connections and layer normalization between them.

To avoid the unexpected interference of target points on observed points and target points themselves, NIERT replaces the original self-attention in the Transformer layer with *partial self-attention* mechanism. As in vanilla self-attention [13], the point embedding h_i^l is firstly transformed to the query vector q_i^l , key vector k_i^l and value vector v_i^l by linear projection matrices W_Q^l, W_K^l, W_V^l , respectively. Then, the unnormalized attention score e_{ij}^l can be computed by scaled dot production of the query q_i^l and key k_j^l :

$$e_{ij}^l = \frac{q_i^l \cdot k_j^l}{\sqrt{d_k}} \quad (1)$$

where d_k is the dimension of the query and key vectors. Unlike the vanilla self-attention layer, we mask out entries of attention weights between target points and all points by replacing these entries with $-\infty$:

$$\hat{e}_{ij} = \begin{cases} -\infty, & \text{if } x_j \in T, \\ e_{ij}, & \text{otherwise} \end{cases}$$

Then the attention score can be obtained by softmax normalization:

$$\alpha_{ij}^l = \frac{\exp(\hat{e}_{ij}^l)}{\sum_p \exp(\hat{e}_{i,p}^l)} \quad (2)$$

In this way, a masked entry α_{ij}^l is equal to 0 when the j -th point is a target point, which is also illustrated in Fig. 2. Then the layer output h_i^{l+1} can be computed as follows:

$$h_i^{l+1} = \text{LayerNorm}(\tilde{v}_i^l + \text{MLP}(\tilde{v}_i^l)), \quad (3)$$

$$\text{where } \tilde{v}_i^l = \text{LayerNorm}\left(v_i^l + \sum_j \alpha_{ij}^l v_j^l\right). \quad (4)$$

Through partial self-attention, for each observed point $(x_j, y_j) \in O$, we maintain α_{ij}^l not masked; thus, NIERT can model the correlation between observed points and target points and the correlation among observed points themselves (Fig. 2). Relatively, the correlation among observed points is easier to learn as these points have known

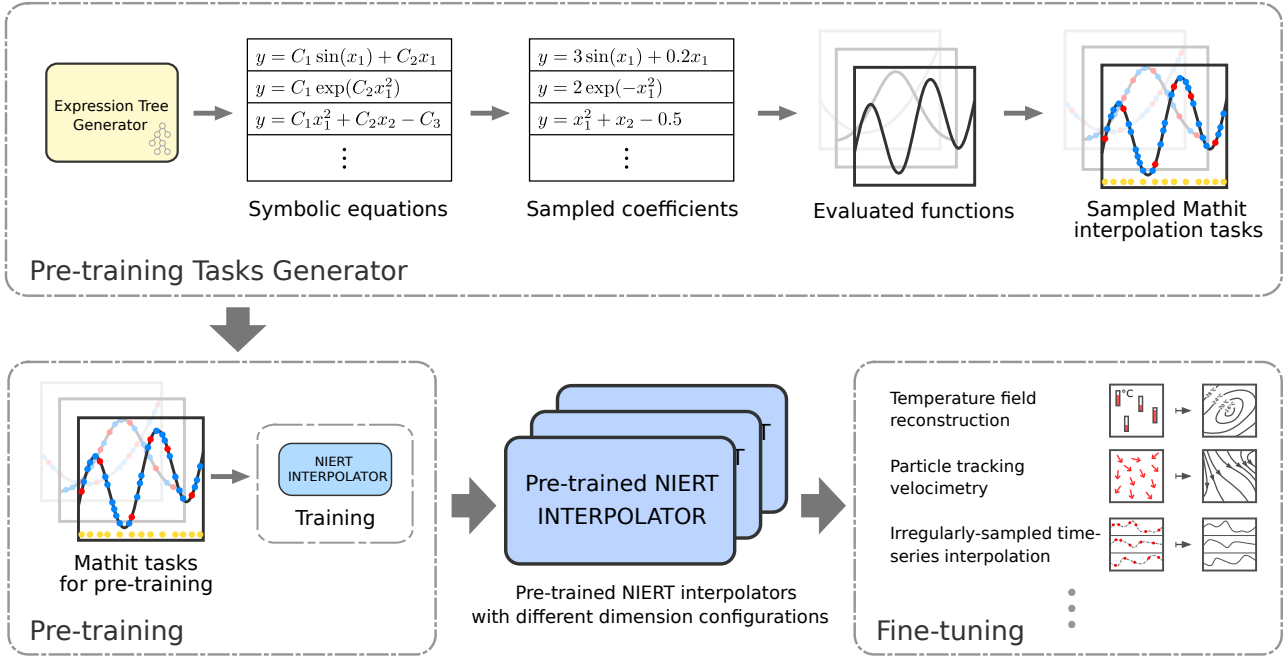


Fig. 3. The generation process of **Mathit** pre-training task set and the pre-training and fine-tuning technique for NIERT interpolator. By randomly sampling the expression trees and coefficients, we synthesized a large number of mathematical functions that can represent a sufficiently wide and diverse function distribution. These functions are evaluated numerically and used to sample the Mathit interpolation tasks used for pre-training. The pre-training introduces prior knowledge into the interpolators and improves their generalization power in various real-world interpolation scenarios.

values. In addition, this correlation can be transferred onto the target points, thus promoting learning representations of these data points. In contrast, by forcing the weight α_{ij}^l to be 0 for each target point j , we completely avoid the unexpected interference of target points on the other points. This design will eventually lead to the more robust representation of the target points and more accurate values will be estimated.

Estimating values for target points. For each target point i , we estimate its value \hat{y}_i through feeding its features at the final Transformer layer into a fully connected feed-forward network, i.e.,

$$\hat{y}_i = \text{MLP}_{\text{out}}(h_i^L).$$

We calculate the error between the estimation and the corresponding ground-truth value, and compose the errors for all points into a loss function \mathcal{L} to be minimized.

3.3 Pre-training NIERT interpolators

We pre-train the NIERT interpolation model to obtain powerful pre-trained interpolators and apply them to various interpolation scenarios (Fig 3). Since the dimension of the input and output of the function, d_x, d_y , which affects the architecture of the interpolator, may be different in various interpolation scenarios, we build a series of pre-trained interpolation models to accommodate scenarios with different function dimensions (d_x, d_y). The pre-trained NIERT in a certain (d_x, d_y) configuration has strong generalization power to different scenarios with the same dimension configuration. For example, the pre-trained NIERT with (2, 1) dimension can be transferred into 3 different subsets of 2D temperature field reconstruction, i.e., HSink, ADlet and

DSine, which are temperature field data for three quite different types of physical conditions [3].

The key to the pre-training process is the construction of the pre-training task set. We propose a **math** function interpolation task set, namely, **Mathit**, for pre-training our model. These tasks for pre-training are sampled from synthesized mathematical functions (see Fig 3). These mathematical functions can be evaluated numerically with perfect accuracy and are suitable for sampling interpolation tasks to train highly accurate interpolators. The configured synthesis process is flexible to generate functions of different dimensions, which are adequate for training interpolator families. Synthesizing data exhibits significant advantages over collecting data from the real world on large scale and at low costs.

TABLE 1
Operators with corresponding sample weights used in generating mathematical functions for pre-training

Operator	+	×	-	. ²	. ³	exp	sin	cos
Sample weight	10	10	5	4	2	4	4	4

Synthesis of mathematical expressions. We borrow the work of [28], [30] to randomly synthesize mathematical functions. A mathematical function is synthesized in the form of an expression tree, where the internal nodes are operators and the leaf nodes are independent variables and coefficients. Eight types of operators with different sampling weights are used in the random synthesis (Table 1), and each synthesized expression have at most 6 operators. We use these operators excluding ‘÷’ or ‘log’, because it should be guaranteed that the synthesized functions are continuous

so as to sample legitimate interpolation tasks. Leaf nodes have a probability of 0.8 to be independent variables and a probability of 0.2 to be coefficients. The optional set of independent variables depends on the dimensionality of the scattered point in the task. For example, when the dimension of the scattered points d_x is 3, the independent variables are chosen with equal probability as x_1, x_2, x_3 . For each dimension of function input d_x , we randomly synthesized one million of these expressions with coefficients and saved them for the subsequent sampling of the interpolation task.

Sampling pre-training interpolation tasks. At training time, the coefficients of each expression are randomly sampled from $[-2, 2]$, such that the functions seen by the model are all different. Once the coefficients in an expression are determined, the expression can be numerically evaluated as a mathematical function. Next, an interpolation task is sampled from each evaluated function. We randomly sample 256 scattered points from within $[-1, 1]^{d_x}$, and compute the values of the function on these points. The function values of the scattered points can be very large or small, which may lead to exploding or vanishing gradients during training, so we normalize the values of each set of scattered points. To construct an interpolation task, we divide these 256 points into n observed points and $256 - n$ target points randomly. Here, we randomly set n to an integer in $[10, 50]$, which induces the generalizability of our model to a variable number of observed points. In this way, an interpolation task for pre-training is sampled.

Dimensional augmentation technique. To synthesize mathematical functions with output dimension greater than 1 ($d_y > 1$), we use the dimensional augmentation technique, which randomly takes d_y functions from the mathematical function set with independent variable dimension d_x and concatenates them together. We do this based on the simple fact that functions of multiple dependent variables can be directly expressed as a combination of multiple functions of one dependent variable. For example, a two-dimensional velocity field can be expressed as $[v_x(x, y), v_y(x, y)]$.

Pre-training and fine-tuning. We pre-train this series of NIERT interpolators separately for different (d_x, d_y) configurations. For a specific (d_x, d_y) configuration, the pre-trained NIERT interpolator can be transferred to different interpolation scenarios of the same dimension configuration. After pre-training, we obtain pre-trained NIERT interpolators with general interpolation capabilities that can be fine-tuned on a domain-specific set of interpolation tasks.

4 EXPERIMENT SETTING

In this section, we present the description of datasets used for our experiments, the baselines used for comparison, and the experimental details.

4.1 Datasets

We evaluate our approach on four representative datasets, including two synthetic datasets and two real-world datasets. These datasets are representatives of interpolation tasks in various application fields: Mathit for mathematical function interpolation, TFRD [3] for temperature field reconstruction, PTV [31] for two-dimensional particle tracking velocimetry, PhysioNet [32] for time-series data interpolation. We introduce each dataset in detail as follows.

1) Synthetic dataset I: Mathit, which denotes the pre-trained dataset we constructed (described in detail in Section 3.3), is used to test the performance for mathematical function interpolation. We evaluate the interpolation accuracy of NIERT and existing approaches on functions of various independent variable dimensions d_x , including 1D, 2D, 3D and 4D. In addition to the pre-trained dataset, we synthesized a test set including 12,000 interpolation tasks for each independent variable dimension of functions. To avoid the intersection between training and test sets, we remove the mathematical expressions appearing in both sets.

2) Synthetic dataset II: TFRD is used to test the performance for 2D temperature field reconstruction. It consists of three sub-datasets with large differences: HSink, ADlet, and DSine, each of which simulates the temperature field of mechanical devices using a specific kind of heat generation and boundary conditions [3]. Each reconstruction task in each subset has 200×200 regular grid points that represent the temperature field in a $0.1m \times 0.1m$ square area. Among these points, 37 scattered points have their temperature known and are used as observed points. The other points are used as target points. In each subset, we have a total of 10,000 training instances and 10,000 test instances. We follow to use L_1 -form loss function for this dataset as performed in [3] for fair a comparison.

3) Real-world dataset I: PTV is a scattered data set where the scattered points are particles with velocities in the flow field. PTV is used to test the performance for particle tracking velocimetry, i.e., the two-dimensional velocity field reconstruction from a finite number of observed particles with velocities. These data are extracted from the raw images of the laminar jet experiment scenes taken by [31]. There are 1200 raw frames in total corresponding to 1200 velocity fields, and each frame extracts a set of scattered points with velocity, which have at most close to 6000 points and at least 2000 points. For each set of scattered data, we randomly take 512 points as observed points and the remaining points as target points to construct an interpolation task. We randomly select a quarter of the tasks as the test set and the rest as the training set.

4) Real-world dataset II: PhysioNet excerpted from the PhysioNet Challenge 2012 [32], is used to test the performance of NIERT for irregularly-sampled time series interpolation. This real-world dataset was collected from intensive care unit (ICU) records. Each instance consists of multiple points, each point represents a measurement of a patient at a specific time, and each measurement contains up to 41 physiological indices. Following the study in [24], we randomly divided the points into observed points and target points, then trained and evaluated interpolation models using the acquired interpolation task sets. We set the ratio of observed points at three levels, i.e., 50%, 70%, and 90% for adequate comparisons. We randomly divided the 8,000 instances of PhysioNet into the training set and test set with a ratio of 4 : 1. Since these time series as functions have a dependent variable of dimension 41, to evaluate the effectiveness of the pre-training on this dataset, we additionally pre-trained a NIERT model suitable for such functions using the dimensional augmentation technique.

We list the statistics of all the above datasets in Table 2. In

TABLE 2
Statistics of the interpolation tasks used for training in each dataset.

Dataset	Subset tag	x 's dimension d_x	y 's dimension d_y	#All points N	#Observed points n	#Target points m
Mathit	1D/2D/3D/4D	1/2/3/4	1	256	[10, 50]	$N - n$
TFRD	ADlet/DSine/HSink	2	1	40000	37	$N - n$
PTV	-	2	2	[2291, 5899]	512	$N - n$
PhysioNet	-	1	41	[20, 190]	$0.5N/0.7N/0.9N$	$N - n$

practice, for each instance in the training set, i.e., N scattered points from a certain function, we randomly select n of them as observed points and the remaining $N - n$ as target points. For the Mathit dataset, we randomly select a fixed range of numbers as the number of observed points (e.g. [5, 50] for Mathit dataset). For the real-world PhysioNet dataset, which has a variable number of scattered points for its instances, distributed in the range of [20, 190], we, therefore, select observed points from all points at a fixed rate (say 50%, 70% or 90%).

4.2 Baselines

All baselines can be divided into two categories: 1) traditional interpolation algorithms and 2) learning-based models.

Traditional Interpolation Algorithms.

Radial basis function (RBF) interpolation is one of the most commonly-used scattered data interpolation methods. It adopts a specific type of radial basis function on observed points and uses their linear combination to represent the target function. We use the RBF interpolation implementation in SciPy [33] and multiquadric function as the basis function type for the experiments.

MIR is another multivariate interpolation and regression method for scattered data sets proposed by [21]. MIR represents the approximation error with Taylor expansions and minimizes the approximation error to find the basis functions.

Learning Based Models.

Conditional neural processes (CNPs) proposed by [9] is a neural model composed of MLPs, which is able to learn to predict distributions of functions given observed points.

Attentive neural processes (ANPs) [10] leverages the attention mechanism in CNPs and improves the prediction performance.

Bootstrapping attentive neural processes (BANPs) [11] employs the bootstrap technique to further improve the performance of ANPs.

TFR-Transformer, proposed in [3], uses Transformer [10] in 2-dimensional temperature field reconstruction using scattered observations.

RNN-VAE is a VAE-based model where the encoder and decoder are standard RNN models. Gated Recurrent Unit (GRU) [34] module is configured as the recurrent network.

L-ODE-RNN refers to the latent neural ODE model where the encoder is an RNN and the decoder is a neural ODE proposed in [35].

L-ODE-ODE refers to the model where the encoder is an ODE-RNN [36] and the decoder is a neural ODE.

mTAND-Full [24] performs time attention mechanism and Bidirectional RNNs to encode temporal features and interpolate irregular-sampled time series data.

TABLE 3
Hyper-parameters of NIERT in experiments on the four datasets.

Parameter name	Parameter value in experiments on			
	Mathit	TFRD	PIV	PhysioNet
x 's embedding dimension	$16 \times d_x$	32	32	16
y 's embedding dimension	16	16	32	592
Number of layers	6	3	3	3
Number of heads	8	4	4	4
Hidden dimension	512	128	128	128

4.3 Experimental details

Model hyper-parameters. Table 3 lists the hyper-parameters of NIERT in the experiments on the four representative datasets, including Mathit, TFRD, PIV and PhysioNet. To fairly evaluate the performance of the pre-trained models, the hyperparameters of the pre-trained models we used on the TFRD, PIV and PhysioNet datasets were aligned with those of NIERT. In addition, we configured the TFR-transformer with the same hyperparameter settings for a fair comparison. For hyperparameter settings of other baselines, we follow the settings in the work of [3] and [24].

Evaluation metrics. For the Mathit, PTV, and PhysioNet datasets, we used the mean square error (MSE) of interpolation on the target points to evaluate the interpolation accuracy of the model. For the TFRD dataset, we follow the work of [3] and used the mean absolute error (MAE) on the target points to evaluate the accuracy of the temperature field reconstruction.

Training details. We used MSE as the loss function for training on Mathit, PTV, and PhysioNet datasets, and MAE as the loss function for training on TFRD dataset, which is consistent with the respective evaluation metric settings. We used Adam for parameter optimization. For pre-training on the Mathit dataset, we sampled mini-batches of size 150 and used a learning rate of 10^{-4} , no schedules, and trained for 160 epochs. For training or fine-tuning on the TFRD, PTV and PhysioNet dataset, we sampled mini-batches of size 5, 32 and 4 respectively. The models were trained on these three datasets using a learning rate of 10^{-4} , and the learning rate was decayed by a factor of 0.97 at the end of each epoch.

5 RESULTS

In this section, we present experimental results and analysis, including interpolation accuracy on synthetic and real-world datasets, individual case studies of interpolation,

TABLE 4
Interpolation accuracy on Mathit dataset.

Interpolation approach	MSE ($\times 10^{-5}$) on Mathit test set			
	1D	2D	3D	4D
RBF	215.439	347.060	443.094	327.775
MIR	67.281	274.601	448.933	342.997
CNP	67.176	248.668	392.348	314.311
ANP	34.558	140.005	206.699	164.751
BANP	14.913	84.187	143.518	140.288
TFR-transformer	15.556	58.569	99.986	90.579
NIERT	8.964	45.319	77.664	72.025

TABLE 5
Interpolation accuracy on TFRD dataset.

Interpolation approach	MAE ($\times 10^{-3}$) on TFRD test set		
	HSink	ADlet	DSine
CNP	204.351	91.782	92.456
ANP	164.491	54.684	58.589
BANP	59.728	28.671	19.107
TFR-transformer	64.987	27.074	29.961
NIERT	23.519	3.473	8.785
NIERT w/ pretraining	15.076	1.897	4.912

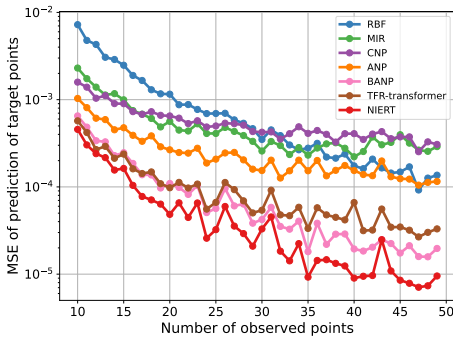
TABLE 6
Interpolation accuracy on PTV dataset.

Interpolation approach	Evaluation criteria
	MSE ($\times 10^{-3}$)
CNP	137.573
ANP	32.111
BANP	33.585
TFR-transformer	17.125
NIERT	5.167
NIERT w/ pretraining	1.954

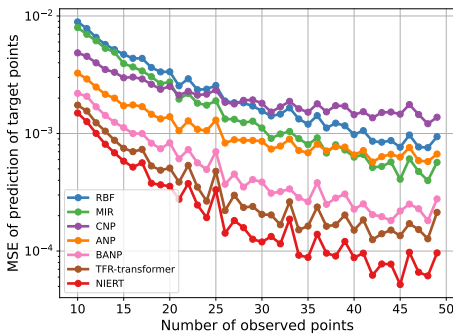
TABLE 7
Interpolation accuracy (MSE, $\times 10^{-3}$) on PhysioNet dataset.

Interpolation approach	Ratio of observed points		
	50%	70%	90%
RNN-VAE	13.418 \pm 0.008	11.887 \pm 0.005	11.470 \pm 0.006
L-ODE-RNN	8.132 \pm 0.020	8.171 \pm 0.030	8.402 \pm 0.022
L-ODE-ODE	6.721 \pm 0.109	6.798 \pm 0.143	7.142 \pm 0.066
mTAND-Full	4.139 \pm 0.029	4.157 \pm 0.053	4.798 \pm 0.036
NIERT	2.868 \pm 0.021	2.656 \pm 0.041	2.709 \pm 0.157
NIERT w/ pretraining	2.831\pm0.021	2.641\pm0.052	2.596\pm0.159

interpretability analysis of attentions, and results of ablation experiments. These results demonstrate the effectiveness and superiority of our approach. We present more results in the Supplementary Material.



(a) On Mathit-1D test set



(b) On Mathit-2D test set

Fig. 4. The relationship between the interpolation accuracy and the number of observed points. Here we use the instances in the Mathit-1D and Mathit-2D test dataset as representatives.

5.1 Interpolation accuracy on synthetic and real-world datasets

For each instance of the test dataset, we applied the trained NIERT and the existing approaches to estimate values for target points. We calculate the mean of errors between estimation and ground truth as interpolation accuracy.

Accuracy on Mathit datasets. As shown in Table 4, on the 1D Mathit test set, RBF shows the largest interpolation error (MSE: 215.439). MIR, another approach using explicit basis functions, also shows a high interpolation error of 67.281. In contrast, BANP and TFR-transformer, which use neural networks to learn interpolation, show relatively lower errors (MSE: 14.913, 15.556). Compared with these approaches, our NIERT approach achieves the best interpolation accuracy (MSE: **8.964** *v.s.* 14.913). Table 4 also demonstrates the significant advantage of NIERT over the existing approach on the 2D, 3D, and 4D instances.

To examine in depth the interpolation accuracy, we further divide test instances into subsets according to the number of observed points. As shown in Fig 4a and Fig 4b, as the number of observed points increases, the interpolation error decreases as expected. In addition, the relative advantages of these approaches vary with the number of observed points, e.g., CNP is better than RBF and MIR initially but finally becomes worse as the number of observed points increases. Among all approaches, NIERT stably shows the best performance over all test subsets, regardless of the number of observed points.

Accuracy on TFRD, PTV and PhysioNet datasets. As shown in Table 5, CNP, although employing the neural network technique, still performs poorly on TFRD datasets. In contrast, NIERT achieves much lower interpolation error (**23.519** *v.s.* 204.351, **3.4739** *v.s.* 91.782 and **8.785** *v.s.* 92.456 on HSink, ADlet and DSink subsets, respectively), which are also significantly lower than ANP, BANP and

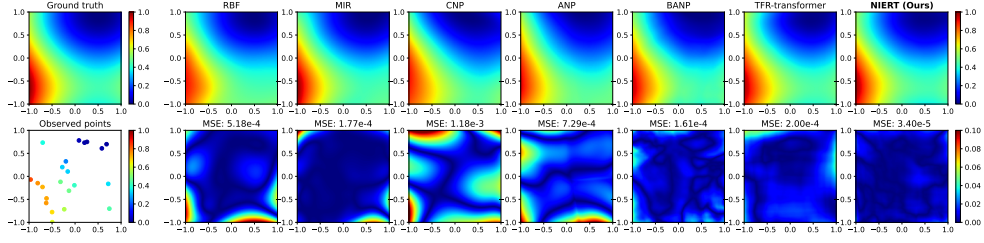


Fig. 5. An example of 2D interpolation task extracted from Mathit test set. The up-left figure shows the ground-truth function $f(x_1, x_2) = 0.65 \cos(1.232 \sin(x_1 + 0.636)) 0.25x_2^2 - 0.25x_2 + 0.156$ while the bottom-left figure shows the 22 observed points. The interpolation functions reported by NIERT and the existing approaches are listed on the top row while their error maps (their differences with the ground truth) are listed below.

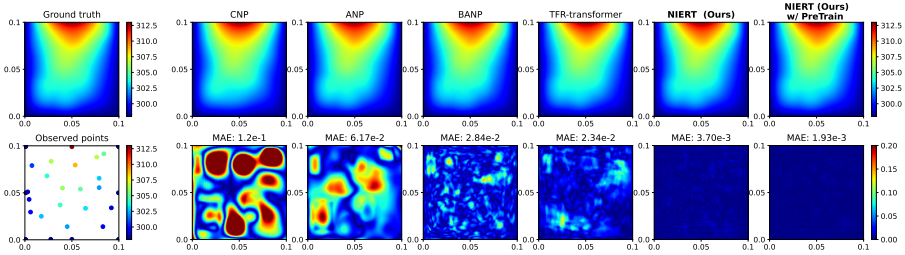


Fig. 6. An example of a temperature field reconstruction task extracted from TFRD-ADlet test set. The up-left figure shows the ground-truth temperature field while the bottom-left figure shows the 32 observed points. The reconstructed results reported by NIERT and the existing approaches are listed on the top row their error maps (their differences with the ground truth) are listed below.

TFR-transformer. Moreover, when enhanced with the pre-training technique, NIERT can consistently further decrease its interpolation MAE by 35%, 45% and 44% relatively on these 3 subsets, respectively, which verifies the strong generalization power of our pre-trained NIERT interpolator.

Table 6 shows that NIERT also outperforms existing methods on the PTV dataset, for example, the average MSE ($\times 10^{-3}$) of NIERT is significantly lower than all other methods (1.954 *v.s.* 17.125). Similarly, the pre-trained NIERT shows better performance. This demonstrates the effectiveness of our NIERT and pre-training method in the 2D particle tracking velocimetry scenario.

Table 7 suggests that on the PhysioNet dataset for irregularly-sampled time series interpolation, NIERT also outperforms the existing approaches, e.g., when controlling the ratio of observed points to be 50%, the interpolation error of NIERT significantly lower than other approaches (2.868 *v.s.* 4.139). Again, NIERT with the pre-training technique shows better performance. The advantages of NIERT hold across various settings of the ratio of the observed points.

Taken together, these results demonstrate the power of NIERT for numerical interpolation in multiple application fields, including mathematical function interpolation, temperature field reconstruction, particle tracking velocimetry, and interpolating irregularly-sampled time-series data. These results also show that the proposed pre-training technique can give NIERT interpolators strong generalization capabilities.

5.2 Case studies of interpolation results

To further understand the advantages of NIERT, we carried out case studies through visualizing the observed points, the reconstructed interpolation functions and the interpolation

errors in this subsection. We have placed an example of Mathit-2D and an example of TFRD-ADlet in Fig. 5 and Fig. 6, respectively. More visualized cases are provided in the Supplementary material.

Fig. 5 shows a 2D instance in the Mathit test set. As illustrated, RBF performs poorly in the application scenario with sparse observed data. In addition, MIR and ANP, cannot accurately predict values for the target points that fall out of the range restricted by observed points. The CNP approach can only learn the rough trend stated by the observed points, thus leading to significant errors. In contrast, BANP, TFR-transformer and NIERT can accurately estimate values for target points within a considerably large range, and compared with BANP and TFR-transformer, NIERT can produce more accurate results.

Fig. 6 shows an instance of temperature field reconstruction extracted from TFRD-ADlet. From this figure, we can observe that NIERT and pre-trained NIERT have significantly lower interpolation errors over the entire region than existing methods. When using the pre-training technique, NIERT further improves its interpolation accuracy in the whole area (with fewer light-colored blobs than non-pre-trained NIERT).

5.3 Interpretability analysis

As demonstrated in Section 3, the partial self-attention mechanism has a good interpretability for the scattered interpolation task, where the attention score indicates the correlation between observed points and the correlation between observed and target points. To analyze the interpretability, we visualized the attention scores in the last attention layer, i.e., α_{ij}^L in Eq. (4), of each observed point to all target points. Here, we take a Mathit-2D interpolation task and set the target points to be points from a 128×128

uniform grid covering the $[-1, 1]^2$ domain, such that these attention weights provide an intuitive description of the contribution by observed points.

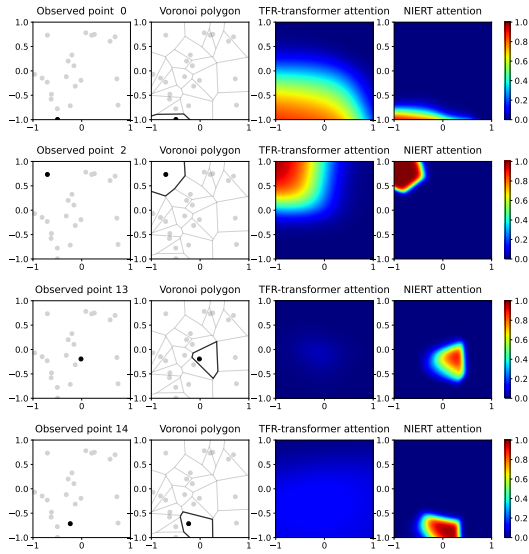


Fig. 7. Contributions of certain observed points for interpolation. We select 4 observed points and extract their attention weights from the final attention layer of NIERT and TFR-transformer. For analysis, we also visualized the Voronoi polygons [37] of the observed points. The contributions by the other 18 observed points are shown in Section 8.3 in the Supplementary material.

As shown in Fig. 7, we compared the attention weights from the final attention layer of NIERT and TFR-transformer. As a reference, we also present the Voronoi polygon [37] corresponding to each observed point, which is exactly the region contributed by each observed point in the nearest neighbor interpolation algorithm. Due to the continuity of the target function, the values of the closer points are close to each other, thus there are strong correlations between such scattered points. Therefore, an ideal highly accurate interpolator should make the observed points tend to affect the target points closer to it rather than more distant ones. Interestingly, we can find that using NIERT, each observed point contributes much more locally and targetedly on an area similar to its Voronoi polygon, which presents a strong interpretability. Moreover, the areas and intensities contributed by each observed point do not overlap exactly with the Voronoi polygon, but are soft and more adaptive. In contrast, when using TFR-transformer, the contributions by observed points are considerably imprecise and imbalanced. These results demonstrate that NIERT has better interpretability and can model the correlation between observed and target points more effectively and accurately.

5.4 Ablation study

The effects of partial self-attention. For a specific interpolation task, the interpolation function is determined by the observed points only. To investigate the effects of partial self-attention in avoiding interference of target points, we evaluated NIERT on the test sets with various numbers of target points. Here, we compared NIERT with its two variants, one using vanilla self-attention, and the other

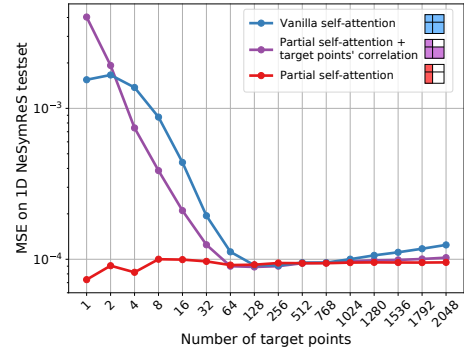


Fig. 8. The robustness of NIERT to the number of target points. Here, NIERT uses three attention mechanisms trained on the Mathit-1D dataset

using partial self-attention with the target points' correlation added. Both of them were trained using the same training sets (the number of target points varies within [206, 246]).

As illustrated by Fig. 8, the two NIERT variants show poor performance for the tasks with few target points, say less than 64 target points or more than 768 target points. In contrast, NIERT, which uses partial self-attention, always performs stably without significant changes in accuracy. The results clearly demonstrate that the partial self-attention mechanism allows NIERT to be free from the unexpected effects of the target points, which enhances the robustness of interpolation.

The effects of pre-training technique. To investigate the effects of the pre-training technique, we show in Fig 9 the training process of two versions of NIERT, one without the pre-training technique, and the other enhanced with pre-training. As depicted by Fig 9a, on TFRD-ADlet dataset, even only after the first epoch, the pre-trained NIERT shows a sufficiently high interpolation accuracy, which is comparable with the fully-trained BANP and TFR-transformer. On PIV dataset (Fig 9b), the pre-trained NIERT has exceeded the final interpolation accuracy of all existing baselines even after the first epoch of fine-tuning. Moreover, the pre-trained NIERT ends up with the smallest interpolation errors on both datasets, which are nearly half of the error of the NIERT without pre-training.

These results suggest that the pre-training technique gives the NIERT interpolator powerful interpolation generalization capabilities. On one hand, it significantly accelerates the convergence and reduces the cost of transfer learning. On the other hand, it improves the final interpolation performance of NIERT.

6 DISCUSSION: CONNECTIONS TO TRADITIONAL APPROACH

The traditional interpolation algorithm constructs the target function as a linear combination of a series of basis functions, usually each of which corresponds to an observed point. For example, to interpolate n observed points $O = \{(x_i, y_i)\}_{i=1}^n$, the RBF approach uses the following

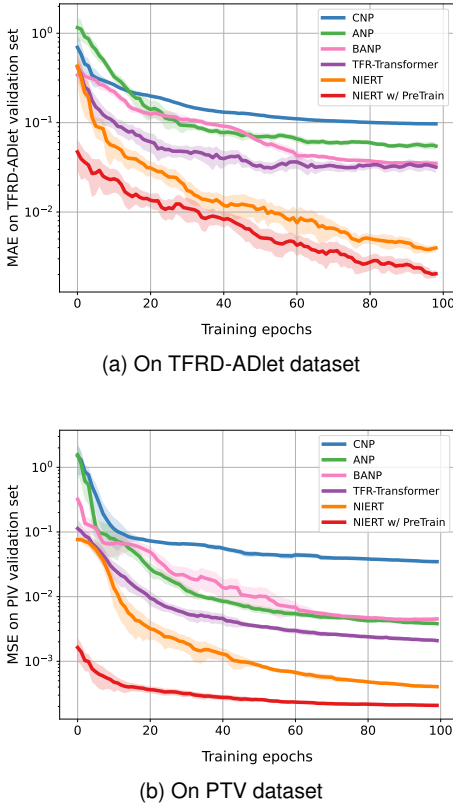


Fig. 9. The convergence of NIERT, NIERT with pre-training, and the existing approaches. Here, these models are trained on TFRD-ADlet and PTV dataset.

interpolation function

$$f_{\text{RBF}}(x) = \sum_{j=1}^n \lambda_j \phi(x, x_j). \quad (5)$$

Here, $\phi(\cdot, x_j)$ represents a radial basis function specified by the observed point x_j , and λ_j is the coefficient, which can be determined through solving the linear equations $\sum_{j=1}^n \lambda_j \phi(x_i, x_j) = y_i, (x_i, y_i) \in O$ [38].

NIERT can be cast as such an instance of interpolation algorithm using basis functions by drawing the following parallels. The core of the NIERT interpolator, i.e., the partial self-attention mechanism shown in Eq. (4) can be rewritten as:

$$f_{\text{Attn}}(x) = \sum_{j=1}^n \alpha(q(x), k_j) v_j. \quad (6)$$

Here, $\alpha(q(x), k_j)$ is the normalized attention weight that models the contribution to query vector $q(x)$ by the key vector k_j , in which k_j and v_j are dominated by the observed point x_j .

Comparing Eq. (5) with Eq. (6), we can find that partial self-attention is a general form of RBF interpolation function: λ_j in Eq. (5) corresponds to v_j in Eq. (6), and $\phi(x, x_j)$ in Eq. (5) corresponds to $\alpha(q(x), k_j)$ in Eq. (6). This correspondence indicates that $\alpha(q(x), k_j)$ can be treated as a learnable basis function and, similarly, v_j can be treated as a predictable basis function coefficient. From this point of view, partial self-attention is a learnable layer that interpolates the representation of observed points to yield

new representations of data points. Together, this insight provides a plausible explanation of the partial self-attention mechanism, which is mutually supportive with the interpretability analysis of the contribution of observed points shown in Section 5.3.

7 CONCLUSION

We present in the study an accurate approach to numerical interpolation for scattered data. The specific features of our NIERT approach are highlighted by the full exploitation of the correlation between observed points and target points through unifying scattered data representation. At the same time, the use of the partial self-attention mechanism can effectively avoid the interference of target points onto the observed points. We also propose to use the large-scale synthesis of generic and diverse mathematical functions to build pre-trained NIERT interpolators with general interpolation capabilities. The advantages of NIERT in interpolation accuracy have been clearly demonstrated by experimental results on both synthetic and real-world datasets. We expect NIERT, with extensions and modifications, to greatly facilitate numerical interpolations in a wide range of engineering and science fields.

ACKNOWLEDGMENTS

We would like to thank the National Key Research and Development Program of China (2020YFA0907000), the National Natural Science Foundation of China (32271297, 62072435, 82130055), and the Leading Innovative and Entrepreneur Team Introduction Program of Zhejiang (2019R02002) for providing financial supports for this study and publication charges.

REFERENCES

- [1] R. Franke and G. M. Nielson, "Scattered data interpolation and applications: A tutorial and survey," *Geometric Modeling*, pp. 131–160, 1991.
- [2] G. Liu, "An overview on meshfree methods: for computational solid mechanics," *International Journal of Computational Methods*, vol. 13, no. 05, p. 1630001, 2016.
- [3] X. Chen, Z. Gong, X. Zhao, W. Zhou, and W. Yao, "A Machine Learning Modelling Benchmark for Temperature Field Reconstruction of Heat-Source Systems," *arXiv preprint arXiv:2108.08298*, 2021.
- [4] D. Dabiri and C. Pecora, *Particle tracking velocimetry*. IOP Publishing Bristol, 2020, vol. 785.
- [5] M. Lepot, J.-B. Aubin, and F. H. Clemens, "Interpolation in time series: An introductory overview of existing methods, their performance criteria and uncertainty assessment," *Water*, vol. 9, no. 10, p. 796, 2017.
- [6] S. N. Shukla and B. M. Marlin, "Interpolation-prediction networks for irregularly sampled time series," *arXiv preprint arXiv:1909.07782*, 2019.
- [7] M. T. Heath, *Scientific Computing: An Introductory Survey, Revised Second Edition*, revised 2nd edition ed. Society for Industrial and Applied Mathematics, 2018.
- [8] R. Bulirsch, J. Stoer, and J. Stoer, *Introduction to numerical analysis*. Springer, 2002, vol. 3.
- [9] M. Garnelo, D. Rosenbaum, C. Maddison, T. Ramalho, D. Saxton, M. Shanahan, Y. W. Teh, D. Rezende, and S. M. A. Eslami, "Conditional Neural Processes," in *Proceedings of the 35th International Conference on Machine Learning*, ser. Proceedings of Machine Learning Research, J. Dy and A. Krause, Eds., vol. 80. PMLR, 10–15 Jul 2018, pp. 1704–1713.

- [10] H. Kim, A. Mnih, J. Schwarz, M. Garnelo, A. Eslami, D. Rosenberg, O. Vinyals, and Y. W. Teh, "Attentive Neural Processes," in *International Conference on Learning Representations*, 2019.
- [11] J. Lee, Y. Lee, J. Kim, E. Yang, S. J. Hwang, and Y. W. Teh, "Bootstrapping neural processes," in *Advances in Neural Information Processing Systems*, H. Larochelle, M. Ranzato, R. Hadsell, M. Balcan, and H. Lin, Eds., vol. 33. Curran Associates, Inc., 2020, pp. 6606–6615.
- [12] B.-J. Lee, S. Hong, and K.-E. Kim, "Residual neural processes," in *Proceedings of the AAAI Conference on Artificial Intelligence*, vol. 34, no. 04, 2020, pp. 4545–4552.
- [13] A. Vaswani, N. Shazeer, N. Parmar, J. Uszkoreit, L. Jones, A. N. Gomez, Ł. Kaiser, and I. Polosukhin, "Attention is all you need," in *Advances in Neural Information Processing Systems*, 2017, pp. 5998–6008.
- [14] J. Devlin, M.-W. Chang, K. Lee, and K. Toutanova, "BERT: Pre-training of deep bidirectional transformers for language understanding," *arXiv preprint arXiv:1810.04805*, 2018.
- [15] H. Bao, L. Dong, and F. Wei, "BEiT: BERT Pre-Training of Image Transformers," *arXiv preprint arXiv:2106.08254*, 2021.
- [16] C. A. Hall and W. W. Meyer, "Optimal error bounds for cubic spline interpolation," *Journal of Approximation Theory*, vol. 16, no. 2, pp. 105–122, 1976.
- [17] W. J. Gordon and J. A. Wixom, "Shepard's method of "metric interpolation" to bivariate and multivariate interpolation," *Mathematics of computation*, vol. 32, no. 141, pp. 253–264, 1978.
- [18] H. Wackernagel, *Multivariate geostatistics: an introduction with applications*. Springer Science & Business Media, 2003.
- [19] M. J. Powell, "Radial basis functions for multivariable interpolation: a review," *Algorithms for approximation*, 1987.
- [20] B. Fornberg and J. Zuev, "The Runge phenomenon and spatially variable shape parameters in RBF interpolation," *Computers & Mathematics with Applications*, vol. 54, no. 3, pp. 379–398, 2007.
- [21] Q. Wang, P. Moin, and G. Iaccarino, "A high order multivariate approximation scheme for scattered data sets," *Journal of Computational Physics*, vol. 229, no. 18, pp. 6343–6361, 2010.
- [22] Y. Tai, J. Yang, and X. Liu, "Image super-resolution via deep recursive residual network," in *Proceedings of the IEEE conference on computer vision and pattern recognition*, 2017, pp. 3147–3155.
- [23] J. Li, Z. Pei, and T. Zeng, "From Beginner to Master: A Survey for Deep Learning-based Single-Image Super-Resolution," *arXiv preprint arXiv:2109.14335*, 2021.
- [24] S. N. Shukla and B. Marlin, "Multi-Time Attention Networks for Irregularly Sampled Time Series," in *International Conference on Learning Representations*, 2021.
- [25] N. Weber, J. Starc, A. Mittal, R. Blanco, and L. Márquez, "Optimizing over a bayesian last layer," in *NeurIPS workshop on Bayesian Deep Learning*, 2018.
- [26] T. Brown, B. Mann, N. Ryder, M. Subbiah, J. D. Kaplan, P. Dhariwal, A. Neelakantan, P. Shyam, G. Sastry, A. Askell, S. Agarwal, A. Herbert-Voss, G. Krueger, T. Henighan, R. Child, A. Ramesh, D. Ziegler, J. Wu, C. Winter, C. Hesse, M. Chen, E. Sigler, M. Litwin, S. Gray, B. Chess, J. Clark, C. Berner, S. McCandlish, A. Radford, I. Sutskever, and D. Amodei, "Language Models are Few-Shot Learners," in *Advances in Neural Information Processing Systems*, H. Larochelle, M. Ranzato, R. Hadsell, M. F. Balcan, and H. Lin, Eds., vol. 33. Curran Associates, Inc., 2020, pp. 1877–1901.
- [27] K. He, X. Chen, S. Xie, Y. Li, P. Dollár, and R. Girshick, "Masked autoencoders are scalable vision learners," *arXiv preprint arXiv:2111.06377*, 2021.
- [28] L. Biggio, T. Bendinelli, A. Neitz, A. Lucchi, and G. Parascandolo, "Neural Symbolic Regression that Scales," in *International Conference on Machine Learning*. PMLR, 2021, pp. 936–945.
- [29] M. Valipour, B. You, M. Panju, and A. Ghodsi, "SymbolicGPT: A Generative Transformer Model for Symbolic Regression," *arXiv preprint arXiv:2106.14131*, 2021.
- [30] G. Lample and F. Charton, "Deep learning for symbolic mathematics," *arXiv preprint arXiv:1912.01412*, 2019.
- [31] A. Sciacchitano, D. R. Neal, B. L. Smith, S. O. Warner, P. P. Vlachos, B. Wieneke, and F. Scarano, "Collaborative framework for piv uncertainty quantification: comparative assessment of methods," *Measurement Science and Technology*, vol. 26, no. 7, p. 074004, 2015.
- [32] I. Silva, G. Moody, D. J. Scott, L. A. Celi, and R. G. Mark, "Predicting in-hospital mortality of icu patients: The physionet/computing in cardiology challenge 2012," in *2012 Computing in Cardiology*. IEEE, 2012, pp. 245–248.
- [33] P. Virtanen, R. Gommers, T. E. Oliphant, M. Haberland, T. Reddy, D. Cournapeau, E. Burovski, P. Peterson, W. Weckesser, J. Bright, S. J. van der Walt, M. Brett, J. Wilson, K. J. Millman, N. Mayorov, A. R. J. Nelson, E. Jones, R. Kern, E. Larson, C. J. Carey, Í. Polat, Y. Feng, E. W. Moore, J. VanderPlas, D. Laxalde, J. Perktold, R. Cimrman, I. Henriksen, E. A. Quintero, C. R. Harris, A. M. Archibald, A. H. Ribeiro, F. Pedregosa, P. van Mulbregt, and SciPy 1.0 Contributors, "SciPy 1.0: Fundamental Algorithms for Scientific Computing in Python," *Nature Methods*, vol. 17, pp. 261–272, 2020.
- [34] J. Chung, C. Gulcehre, K. Cho, and Y. Bengio, "Empirical evaluation of gated recurrent neural networks on sequence modeling," *arXiv preprint arXiv:1412.3555*, 2014.
- [35] R. T. Q. Chen, Y. Rubanova, J. Bettencourt, and D. Duvenaud, "Neural Ordinary Differential Equations," *Advances in Neural Information Processing Systems*, 2018.
- [36] Y. Rubanova, R. T. Q. Chen, and D. K. Duvenaud, "Latent Ordinary Differential Equations for Irregularly-Sampled Time Series," in *Advances in Neural Information Processing Systems*, H. Wallach, H. Larochelle, A. Beygelzimer, F. d'Alché-Buc, E. Fox, and R. Garnett, Eds., vol. 32. Curran Associates, Inc., 2019.
- [37] F. Aurenhammer, "Voronoi diagrams—a survey of a fundamental geometric data structure," *ACM Computing Surveys (CSUR)*, vol. 23, no. 3, pp. 345–405, 1991.
- [38] J. Solomon, *Numerical algorithms: methods for computer vision, machine learning, and graphics*. CRC press, 2015.



Shizhe Ding is currently pursuing his Ph.D. degree in the Institute of Computing Technology (ICT), Chinese Academy of Sciences (CAS), Beijing, China. He received his B.E. degree from University of Chinese Academy of Sciences in 2019. His research interests lie in data mining and deep Learning.



Boyang Xia received B.S. degree in 2020 from Beijing University of Posts and Telecommunications. He is currently a master candidate of the Institute of Computing Technology (ICT), Chinese Academy of Sciences (CAS). His research interests include deep learning and computer vision.



Milong Ren received B.S. degree from Shandong University in 2021. He is currently pursuing his Ph.D. degree in the Institute of Computing Technology (ICT), Chinese Academy of Sciences (CAS). His research interests include deep learning and bioinformatics.



Dongbo Bu received his Ph. D. degree from the Institute of Computing Technology (ICT), Chinese Academy of Sciences (CAS). He is now a professor at the institute and his research interests include AI-aided algorithm design, algorithms for protein structure prediction and protein design. He worked with his colleagues to develop ProFOLD, a software for protein structure prediction, ProDESIGN, a software for protein design, and AIA-ILP, a software for solving integer linear programming with aid of AI.

8 ADDITIONAL EXPERIMENTAL RESULTS

8.1 Additional ablation studies

8.1.1 The effects of different model depths

We carried out experiments on Mathit-2D dataset using NIERT with hyper-parameter L varying from 3 to 7. Then evaluate the models on the Mathit-2D test dataset. The accuracy is listed in Table 8. The results show that NIERT with 7 transformer layers has the best accuracy on the test set, and NIERT with 6 transformer layers has reached a comparable level. Therefore, in the experiments on Mathit data set, we use $L = 6$ to balance efficiency and accuracy.

TABLE 8

The interpolation accuracy of NIERT ($\text{MSE} \times 10^{-5}$) under various settings of transformer layer number L on Mathit-2D dataset

Interpolation approach	Number of transformer layers L				
	3	4	5	6	7
NIERT	66.812	60.133	52.098	45.319	44.043

8.1.2 The effects of different hidden dimensions

We also carried out experiments on the Mathit-2D dataset using NIERT with smaller hidden dimensions d_{model} , say from 256, 128 and 64. Then evaluate the models on the Mathit-2D test dataset. The accuracy is listed in Table 9. The results show that when the hidden dimension is within 512, NIERT’s interpolation accuracy is higher when the hidden dimension is larger.

In this experiment, we fix other super parameters, say model depth L as 6 and number of heads as 8.

TABLE 9

The interpolation accuracy of NIERT ($\text{MSE} \times 10^{-5}$) under various settings of hidden dimension d_{model} on Mathit-2D dataset

Interpolation approach	Different hidden dimensions d_{model}			
	64	128	256	512
NIERT	106.193	72.107	51.153	45.319

8.1.3 The effects of prediction error of observed points in loss function

To verify the contribution of re-predicting values of the observed points to the interpolation task, we conducted an experiment that puts the prediction error of observed points in the loss function, i.e. only minimizes the estimation error of target points. The results are shown in Table 10 which demonstrates that only minimizing estimation error of target points make NIERT performing poorly. This indicates that re-predicting the value of observed points helps NIERT to predict the value of target points more accurately.

TABLE 10

Interpolation accuracy ($\text{MSE} \times 10^{-5}$) of NIERT trained with loss only containing the prediction error of the target points

Loss contains prediction error of	Only target points	All points
MSE ($\times 10^{-5}$)	48.931	45.319

8.2 Additional case studies

Cases from Mathit-1D & Mathit-2D test set

In each following example of 1D interpolation task extracted from Mathit test set, the blue curve represents the ground-truth function while the red curves represent the interpolation functions reported by NIERT and the existing approaches.

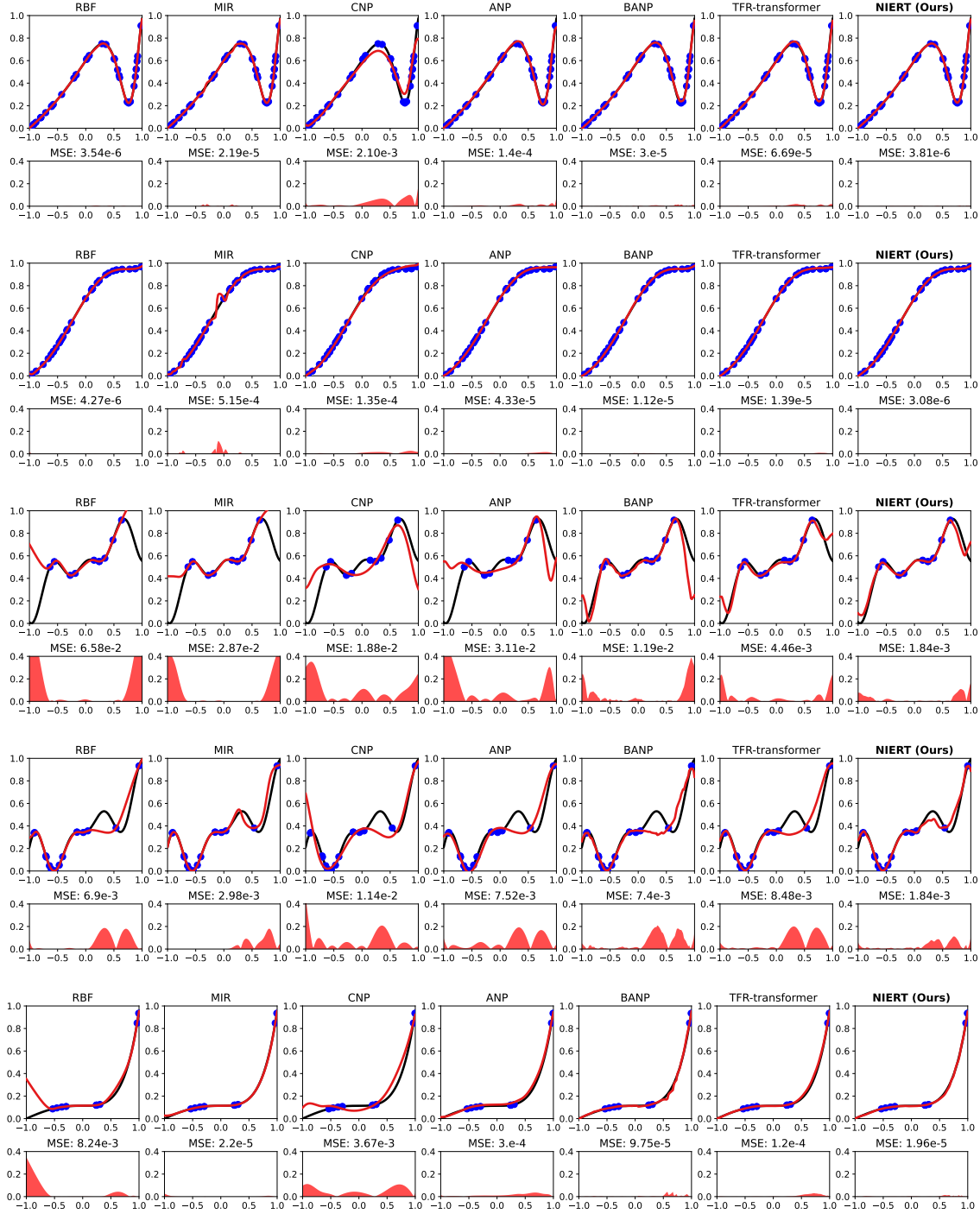


Fig. 10. Additional cases from MathIT-1D test set

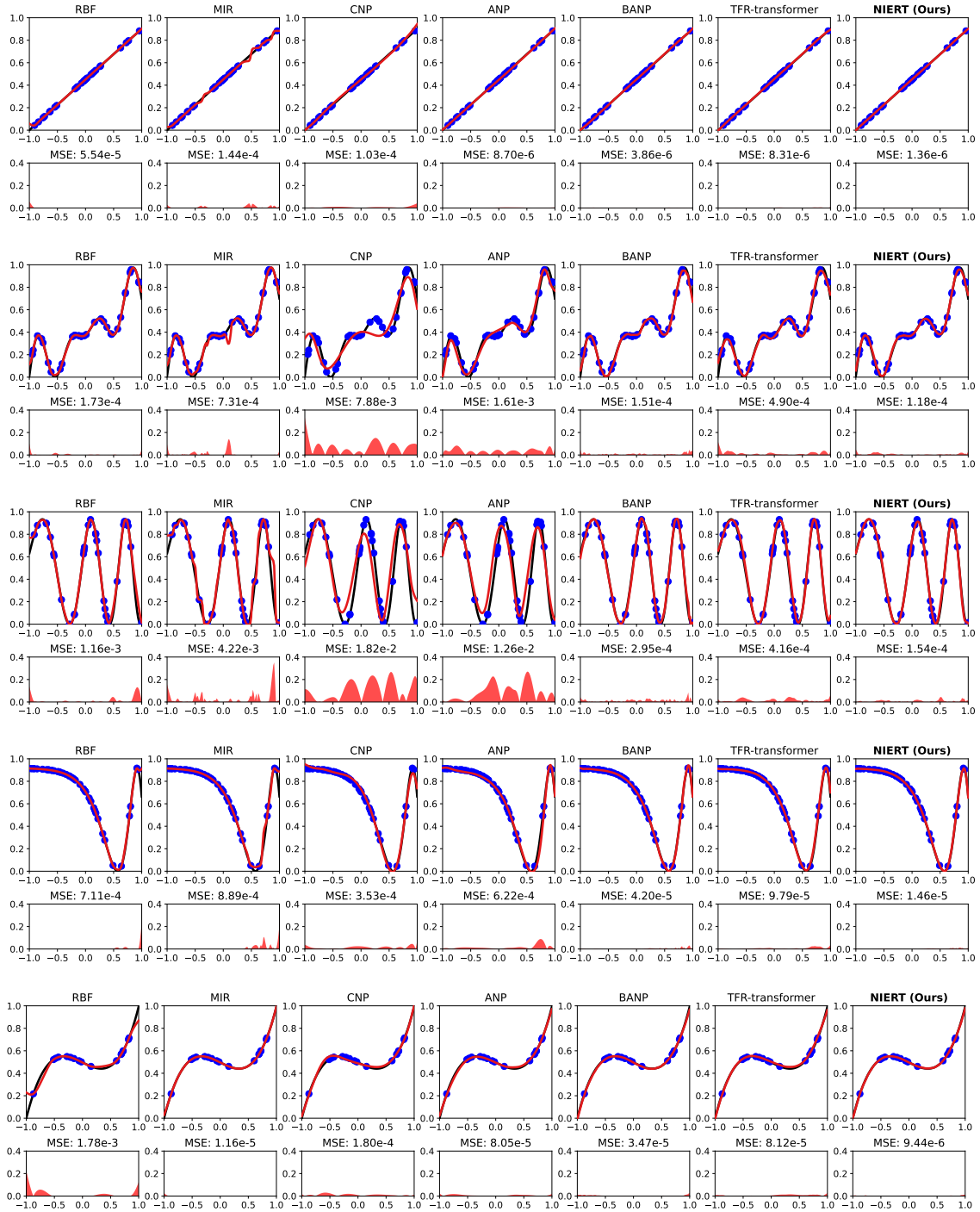


Fig. 11. Additional cases from MathIT-1D test set

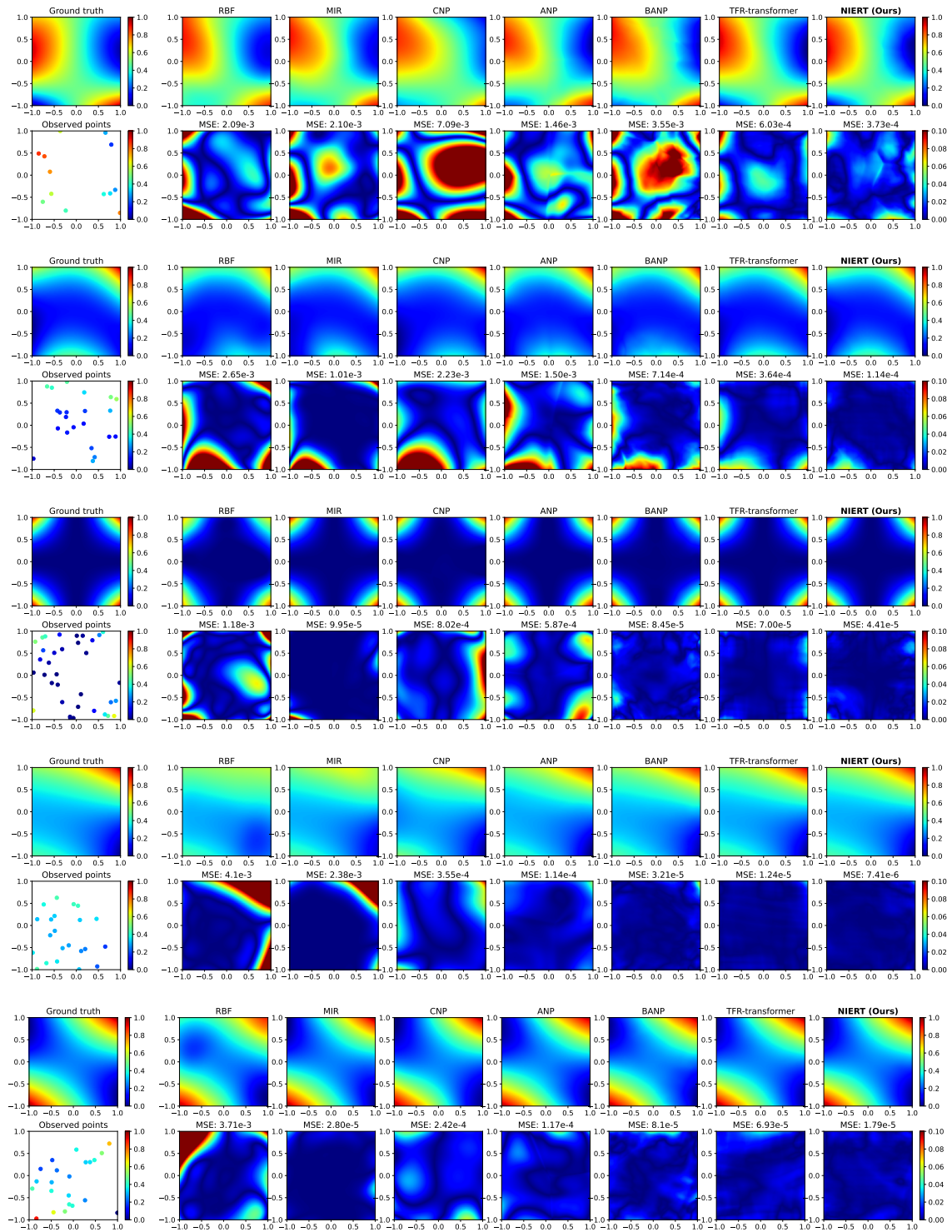


Fig. 12. Additional cases from MathIT-2D test set

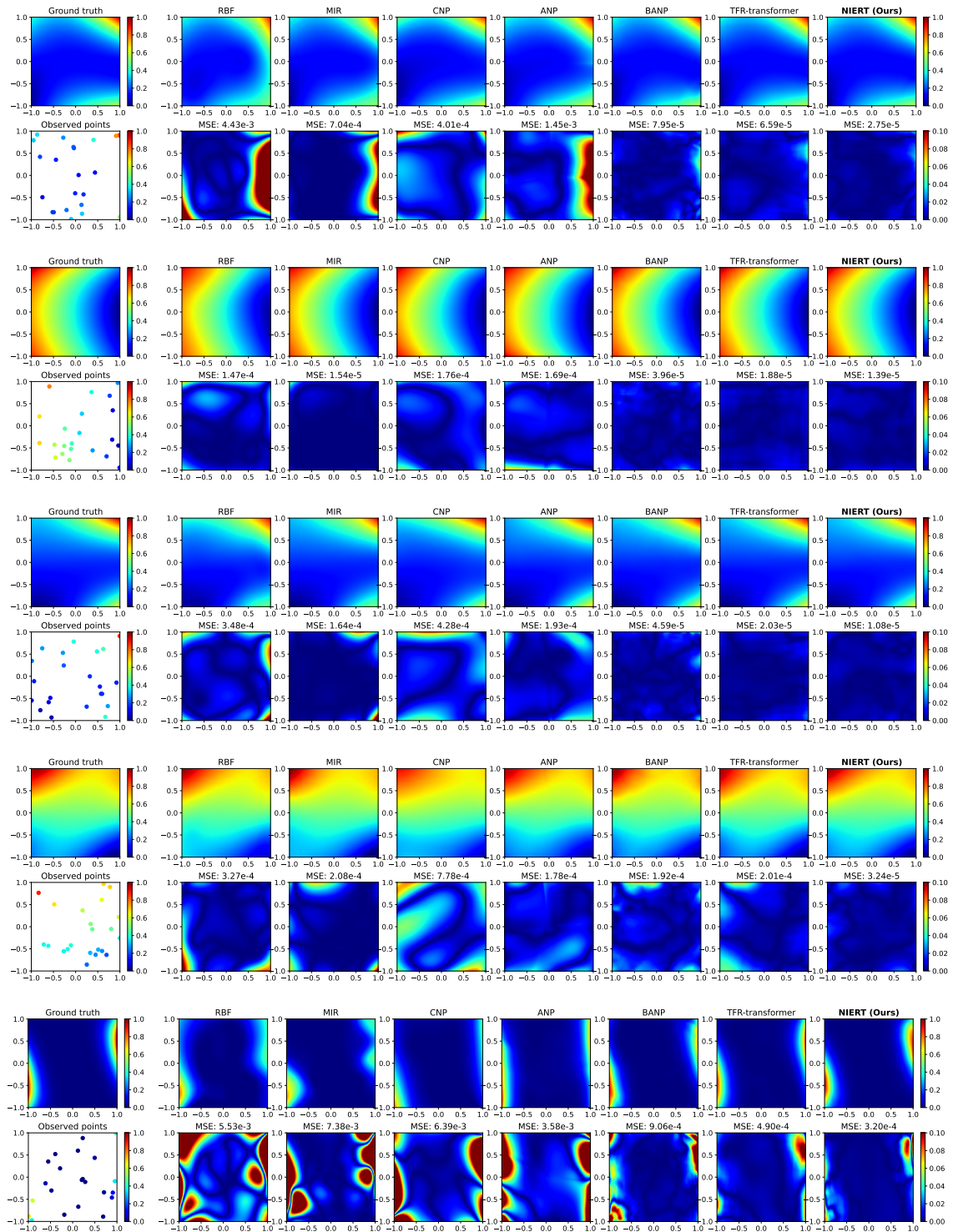


Fig. 13. Additional cases from MathIT-2D test set

Cases from TFRD-HSink

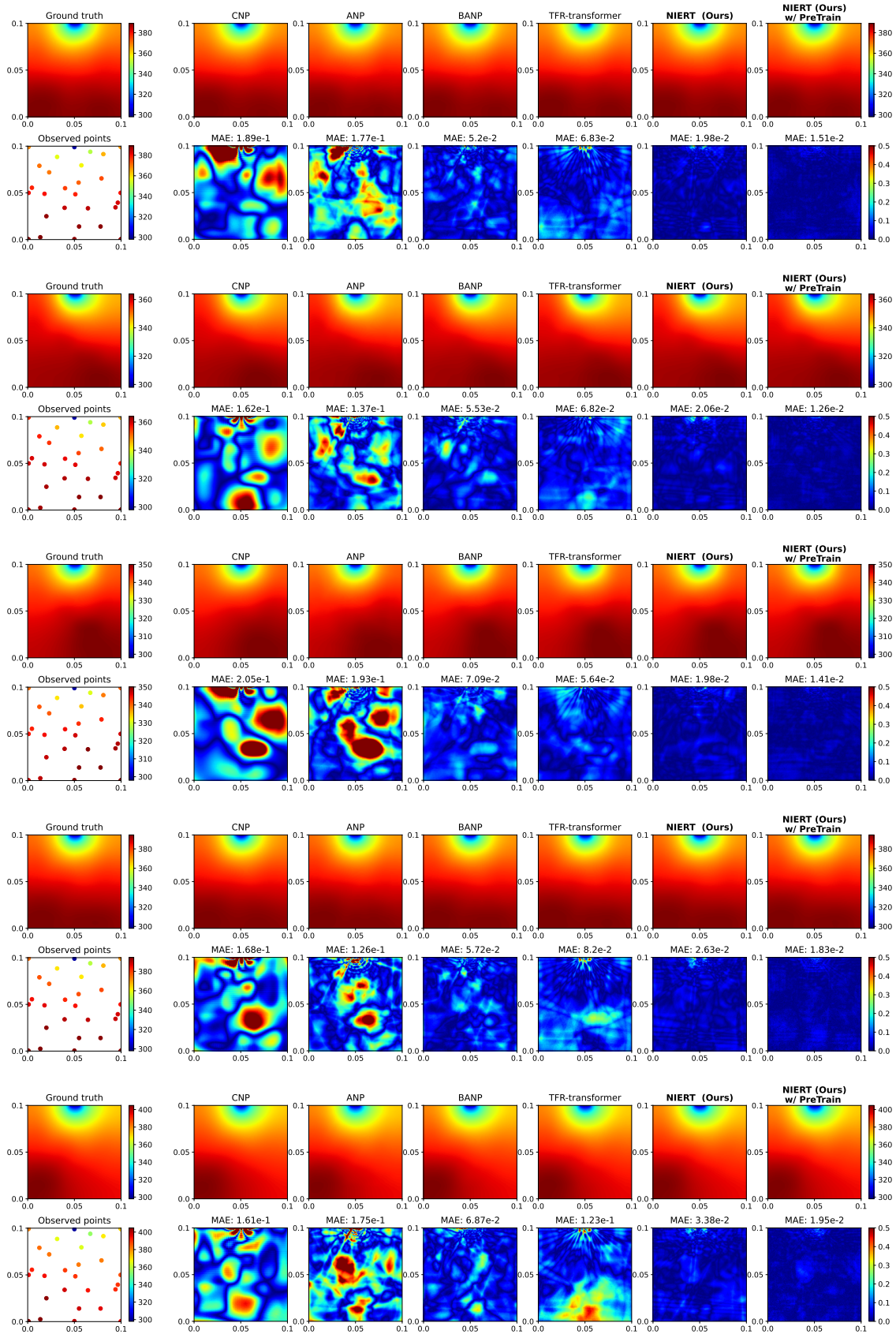


Fig. 14. Additional cases from TFRD-HSink test set

Cases from TFRD-ADlet

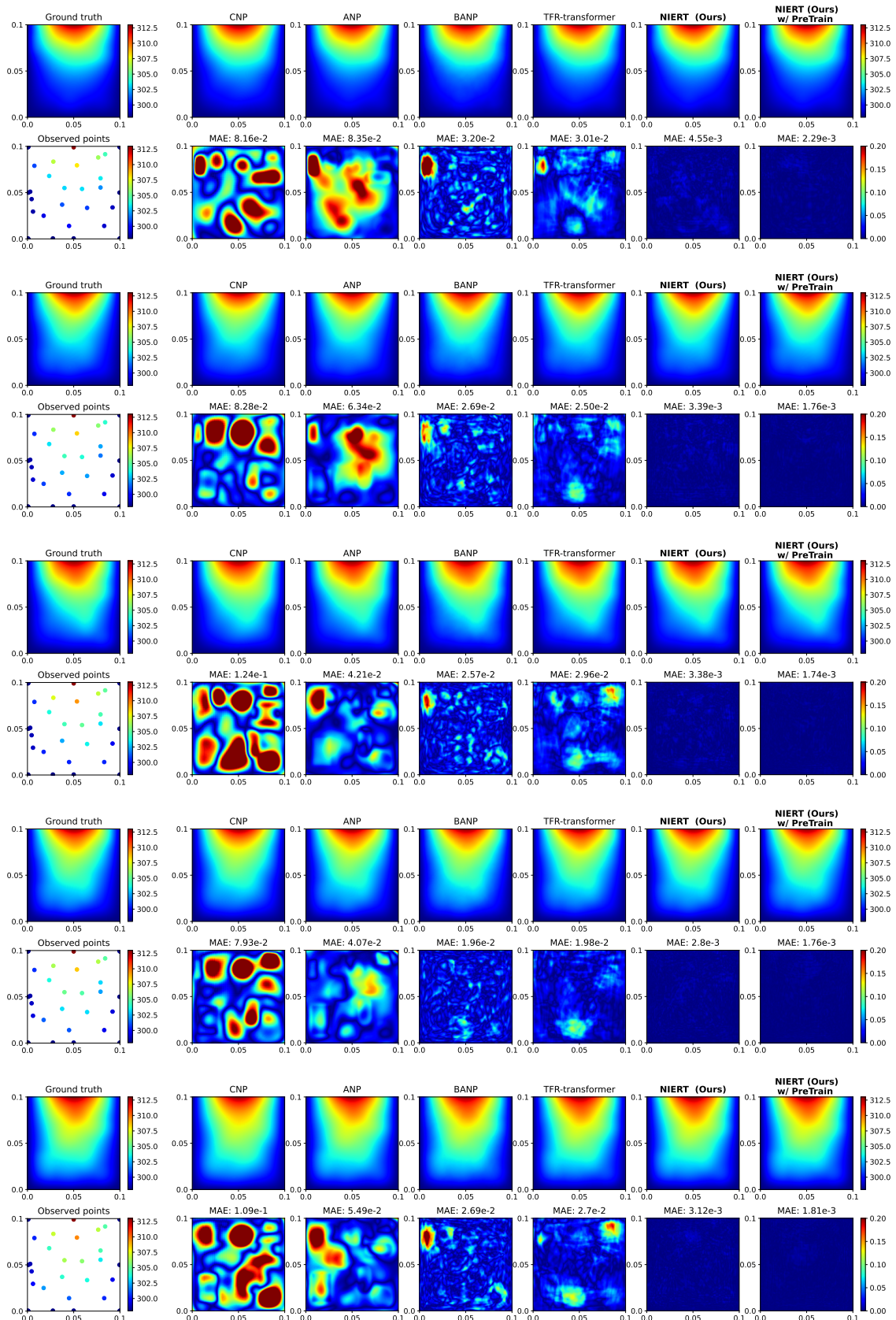
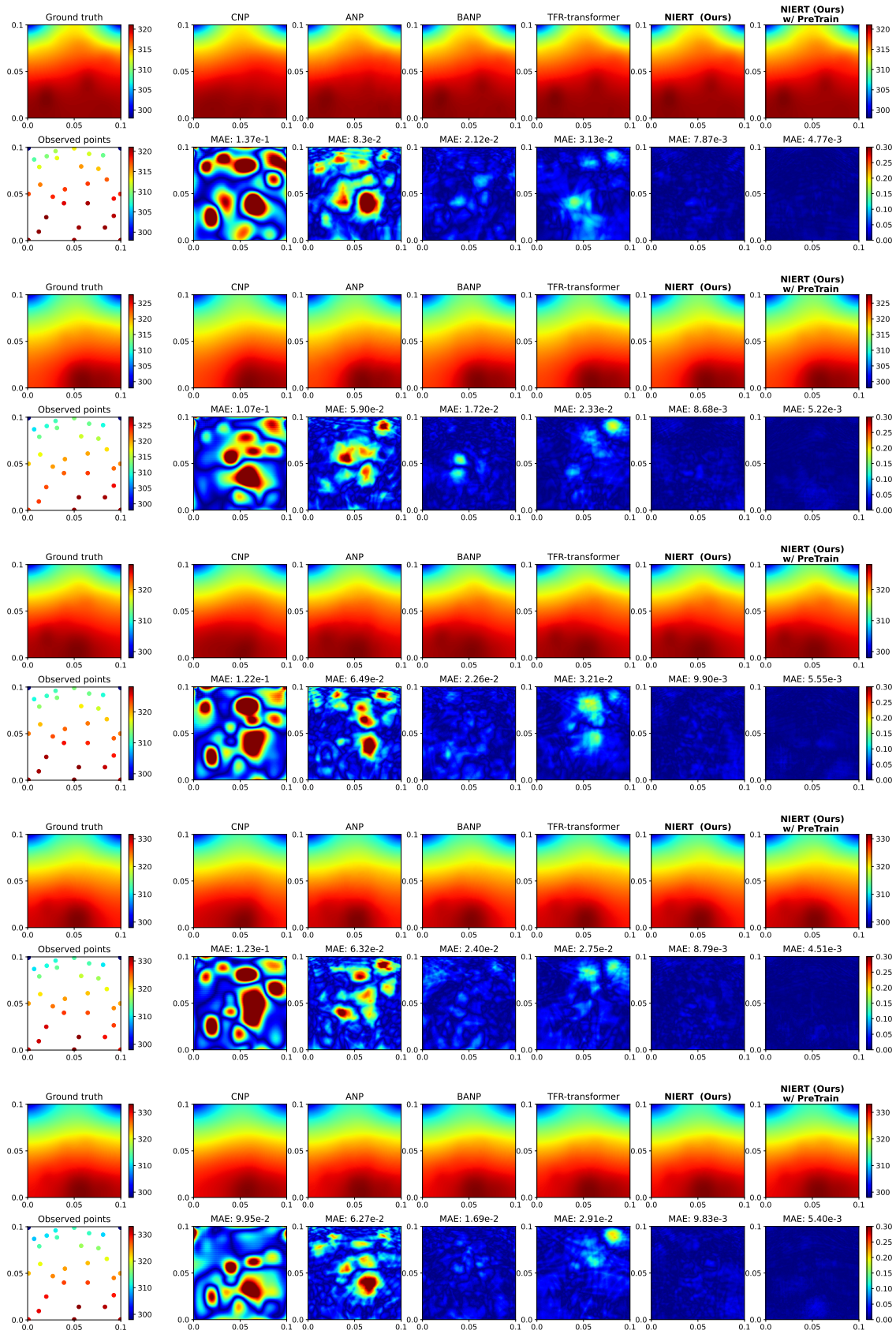


Fig. 15. Additional cases from TFRD-ADlet test set

Cases from TFRD-DSine



PIV

Fig. 16. Additional cases from TFRD-DSine test set

Cases from PTV

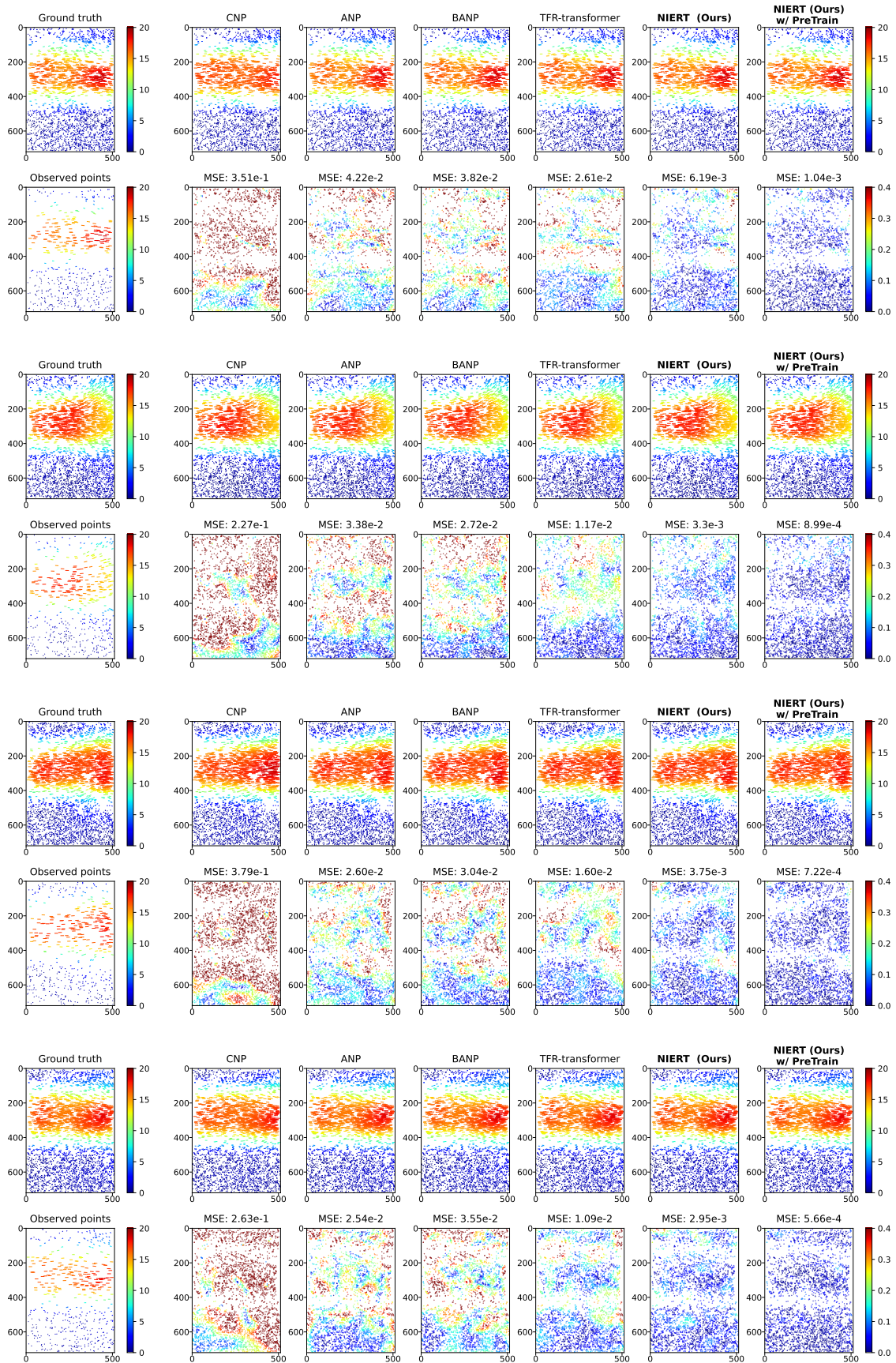


Fig. 17. Additional cases from PTV test set

8.3 Contribution analysis of observed points for interpolation

As supplements to Figure 6, all observed points' attention weights extracted from the final attention layer of NIERT and TFR-transformer are visualized in Figure 18.

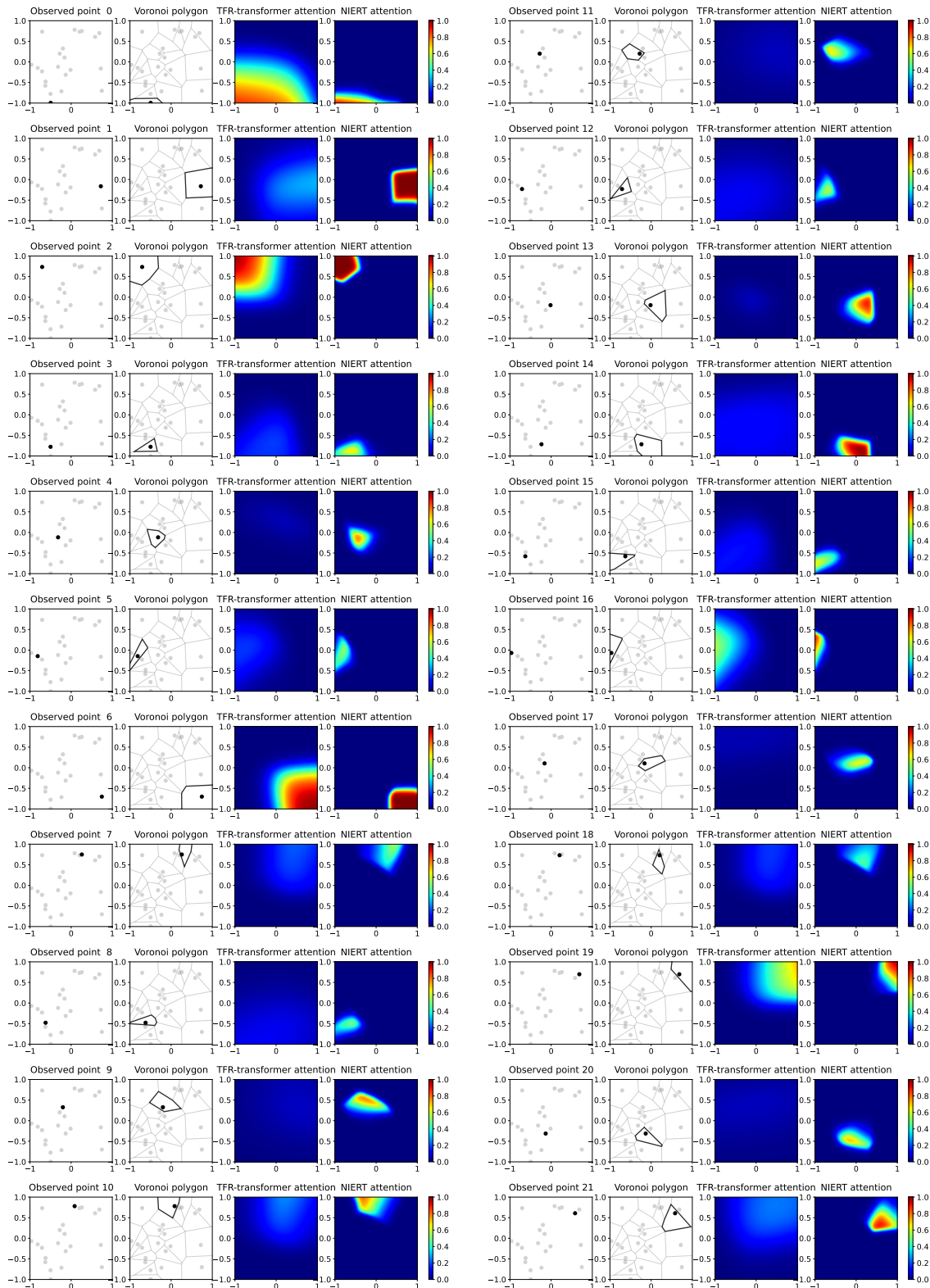


Fig. 18. All observed points and the corresponding extracted attention response

The contributions by observed points are quite imbalanced using TFR-transformer. In particular, the intensity and area of the contributions of the five observed points 0,2,6,16,19 cover almost the entire domain, while the remaining 17 observed points only produce negligible contribution. In contrast, when using NIERT, contributions by an observed point are much

more local and thus targeted and all observed points have contributions to interpolation. This shows that NIERT can fully exploit the relationship between observed points and target points.